metals

MDPI

Article

Effect of Austenite Grain Size on the Bainitic Transformation in a 690 MPa Grade High-Strength Multi-Functional Construction Steel

Zhenye Chen [1,2], Xiujuan Zhao [3,*], Jianjun Qi [1], Wenting Zhu [2], Yanqing Zhao [1] and Liqing Chen [2,*]

[1] Iron and Steel Technology Research Institute, HeSteel Group Co., Ltd., Shijiazhuang 050023, China; chenzhenye@hbisco.com (Z.C.); qijianjun01@hbisco.com (J.Q.); zhaoyanqing@hbisco.com (Y.Z.)
[2] State Key Laboratory of Rolling and Automation, Northeastern University, Shenyang 110819, China; wentingzhu@stumail.neu.edu.cn
[3] Department of Materials Engineering, Hebei Vocational University of Industry and Technology, Shijiazhuang 050091, China
* Correspondence: shishuai@hbisco.com (X.Z.); lqchen@mail.neu.edu.cn (L.C.); Tel.: +86-311-86510869 (X.Z.); +86-24-83681819 (L.C.)

Abstract: A high-strength low-carbon construction structural steel was investigated in the laboratory. The various austenite grain sizes were obtained by austenitizing the steel at different temperatures. The effect of austenite grain size on bainite transformation was studied by the dilatometer. The results show that the microstructure of high-strength low-carbon structural steels mainly includes granular bainite, lath-like bainite and martensite-austenite (M-A). The microstructure changes from granular bainite to lath-like bainite with the increase in austenitizing temperature or austenite grain size. When the samples were heated at the lower temperature of 860 °C, the bainite starting temperature was relatively high, which was mainly attributed to the promotion of the granular bainitic nucleation and the formation of the solute-depleted regions in the austenite. Compared to 860 and 1260 °C, the bainite transformation rate in the specimen austenitized at 1000 °C is the highest because of the small prior austenite grain size and larger transformation driving force.

Keywords: structural steel; microstructure; bainite transformation; austenite grain size; austenitizing temperature

check for updates

Citation: Chen, Z.; Zhao, X.; Qi, J.; Zhu, W.; Zhao, Y.; Chen, L. Effect of Austenite Grain Size on the Bainitic Transformation in a 690 MPa Grade High-Strength Multi-Functional Construction Steel. *Metals* **2022**, *12*, 577. https://doi.org/10.3390/met12040577

Academic Editor: Hardy Mohrbacher

Received: 23 February 2022
Accepted: 27 March 2022
Published: 29 March 2022

Publisher's Note: MDPI stays neutral with regard to jurisdictional claims in published maps and institutional affiliations.

Copyright: © 2022 by the authors. Licensee MDPI, Basel, Switzerland. This article is an open access article distributed under the terms and conditions of the Creative Commons Attribution (CC BY) license (https://creativecommons.org/licenses/by/4.0/).

1. Introduction

The steel structure has many merits in high strength, high load-bearing capacity, lightweight, good reliability, simple construction and low environmental pollution. Since its birth in Europe in the 1950s, it has been used to replace reinforced concrete structures in many countries, and has become the mainstream of the future development of building structures [1–3]. With the advancement of building technology and the escalation in demand, steel structure building has put forward a variety of functions such as high strength, earthquake resistance, fire resistance and corrosion resistance, and there is a tendency to concentrate the multi-function in one type of steel. A hot-rolled low-carbon microalloyed steel with a yield strength of 690 MPa for construction was developed by the authors. This newly developed steel has high strength, low yield ratio, excellent toughness, good fire resistance and corrosion resistance.

The newly developed 690 MPa grade structural steel is a microalloyed steel. One of the advantages of using microalloying elements is the grain refinement caused by the pinning effect of nitrides or carbides of fine microalloys (Nb, V, Ti) [4,5]. Mastering the law of solid-phase transformation is very important for the microstructure design and the optimization of mechanical properties of steels [6,7]. Bainite is a main component in the microstructure of the newly developed 690 MPa grade steel. Therefore, it is necessary to understand the bainite transformation kinetics and related microstructure evolution

in the newly developed structural steel. There are many factors affecting the transformation kinetics of bainite, including carbon content, alloy composition, austenite grain size, austenitization temperature and plastic deformation of austenite. Girault et al. [8] pointed out that the total bainitic transformation kinetics is directly related to austenitizing temperature. Umemoto et al. [9] and Lee et al. [10] believed that the bainite reaction rate was inversely proportional to the austenite grain size (AGS). Lan et al. [11] reported that the volume fraction of bainite increases with the decrease of AGS in a 0.06C-0.30Si-1.71Mn-0.22Cr-0.23Cu-0.21Mo-0.32Ni-0.04V-0.028Nb steel, whereas a coarse austenite grain hinders the isothermal bainitic transformation. Li et al. [12] also found that the decrease of AGS reduces the activation energy of bainitic transformation and accelerates the transformation kinetics. However, Xu et al. [13] and Hu et al. [14] emphasized that coarse austenite grains would lead to an increase in the bainite transformation rate. This is because coarse austenite grains provide fewer nucleation sites and create favorable conditions for bainite growth. Hasan et al. [15] also found that the volume fraction of bainite increases with increasing austenitization temperature. In addition, Matsuzaki and Bhadeshia [16] confirmed experimentally that the AGS has opposite effects on bainite reaction rate of different steels. Taking into account the morphology of bainite, they also derived a general equation describing the rate of the reaction. Their study showed that the refinement of AGS accelerates the bainite transformation kinetics when the bainite growth rate is slow. By contrast, the refinement of AGS retards the transformation kinetics when the bainite growth rate is rapid and the nucleation site is limited. Some scholars pointed out that under continuous cooling conditions, austenite grain size has no significant influence on bainite transition temperature [17–20]. In conclusion, the effect of austenite grain size on bainite transformation kinetics is still controversial.

The purpose of this work is to study the detailed relationship between austenite grain size and bainite transformation dynamics during continuous cooling of high-strength low-carbon construction structural steel.

2. Materials and Methods

The experimental material was a novel 690 MPa grade high-strength multi-functional construction structural steel recently developed by the authors [21]. The chemical composition of the experimental steel is shown in Table 1. The steel was cast into a 50 kg ingot in a vacuum induction furnace (Shenyang Institute of Vacuum Technology, Shenyang, China) and then hot forged into a square billet with a size of 70 mm × 70 mm × 110 mm. The forged slabs were first reheated to 1230 °C and held for 3.5 h. Then, the two-stage controlled rolling was conducted on a 4-high reversible rolling mill (Wuxi Guancheng Metal Technology Co., Ltd., Wuxi, China). In the first stage of controlled rolling, the slab was rolled 4 passes at 1075–1052 °C. In the second stage, the plate steel was rolled 9 passes in the range of 930–880 °C. Finally, 20 mm thick steel plates were obtained. After hot-rolling, the steel plates were air-cooled to 780 °C, then rapidly cooled to 480 °C by an ultra-fast cooling (UFC) system (Northeastern University, Shenyang, China), and finally air-cooled to the room temperature.

Table 1. Chemical composition of the experimental steel (wt.%).

C	Si	Mn	Cu + Cr + Ni	Mo	Ti	Nb + V	N + B	P	S	Fe
0.08	0.28	1.1	1.1	0.4	0.04	0.07	0.006	0.007	0.0017	Bal.

The yield strength, tensile strength, total elongation, and yield ratio of the hot-rolled steel at room temperature are 700 MPa, 878 MPa, 20%, and 0.80, respectively, and this steel possesses good low-temperature toughness. In addition, the steel shows good fire resistance and corrosion resistance. More detailed information on the studied steel can be found in reference [21].

The samples were cut from the center of the steel plate and machined into cylinders of 4 mm in diameter and 10 mm in height. The specimens were heated to the temperatures of 1250 °C, 1000 °C and 860 °C, respectively, with the heating rate of 20 °C/s to obtain different austenite grain sizes. The A_{e3} temperature of the experimental steel was calculated to be approximately 840 °C using the JMatPro 9.0 software (Sente Software Ltd., London, UK), so the minimum reheating temperature was selected to be 860 °C. In addition, 1000 and 1250 °C are selected to obtain prior austenite grains with significantly different sizes. Figure 1 shows the detailed simulated heat treatment process of the specimens, which was carried out using the Formastor-FII machine (FUJI KIKO Co., Ltd., Kosai, Japan). Each sample was held at the peak temperature for 5 s to obtain full austenitization. Then, they were cooled from the peak temperature to 800 °C at a rate of 60 °C/s, followed by cooling to room temperature at a rate of 10 °C/s. It is believed that no transformation from austenite occurred during the rapid-cooling stage to 800 °C because of the high cooling rate and the small undercooling. The changes of sample length throughout the heat treatment process were recorded. After the thermal simulation tests, each specimen was cut into three parts. The first part was etched via the saturated aqueous picric acid at 70 °C in a water bath to reveal the austenite grain. The second part was polished and etched in 4 vol% nital solution at room temperature. Then the microstructures of the specimens were observed by an OLYMPUS BX 53 MRF optical microscope (OM, OLYMPUS, Tokyo, Japan). The third part was polished and etched with LePera reagent in order to reveal the morphology of the M-A constituents. The prior austenite grain sizes were quantified using the linear intercept method.

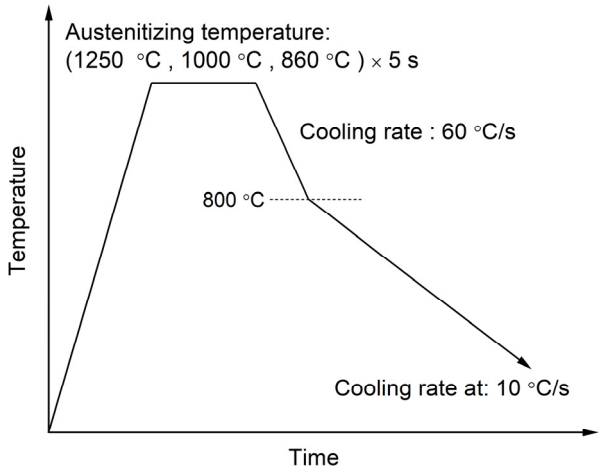


Figure 1. Schematic of the simulated heat treating process with different austenitization temperatures.

3. Results and Discussion

3.1. Microstructure

Figure 2 shows the microstructures of the newly designed experimental steel with different austenitization temperatures. The average AGS was increased from 7 to 62 μm as the austenitization temperature increased from 860 °C to 1250 °C. When the experimental steel was austenitized at 860 °C, the microstructure consists of typical granular bainite and a few polygonal ferrite (Figure 2a). As shown in Figure 3a, blocky martensite and small martensite-austenite (M-A) constituents form along grain boundaries and appear white after being etched with LePera reagent. When the austenitization temperature was increased to 1000 °C, a visible number of lath bainite (or bainite ferrite), granular bainite and a small amount of M-A constituents were generated in the microstructure, as shown in Figures 2b and 3b. In addition, compared to the specimen austenitized at 860 °C, the austenite grains do not coarsen significantly at 1000 °C due to the pinning effect of fine precipitates which do not fully dissolve into the matrix. Bainite can only grow inside the austenite grain due to the ledge growth mechanism and displacive mechanism, so the

austenite grain boundaries in the microstructure are clear and complete [22–24]. When the austenitization temperature was 1250 °C, the microstructure of the sample changed into a mixture of lath bainite and lath martensite, and the prior austenite grains grew abnormally (Figures 2c and 3c). In summary, the morphology of the microstructure changes from polygonal ferrite and granular bainite to lath bainite as the austenitizing temperature is increased from 860 to 1250 °C.

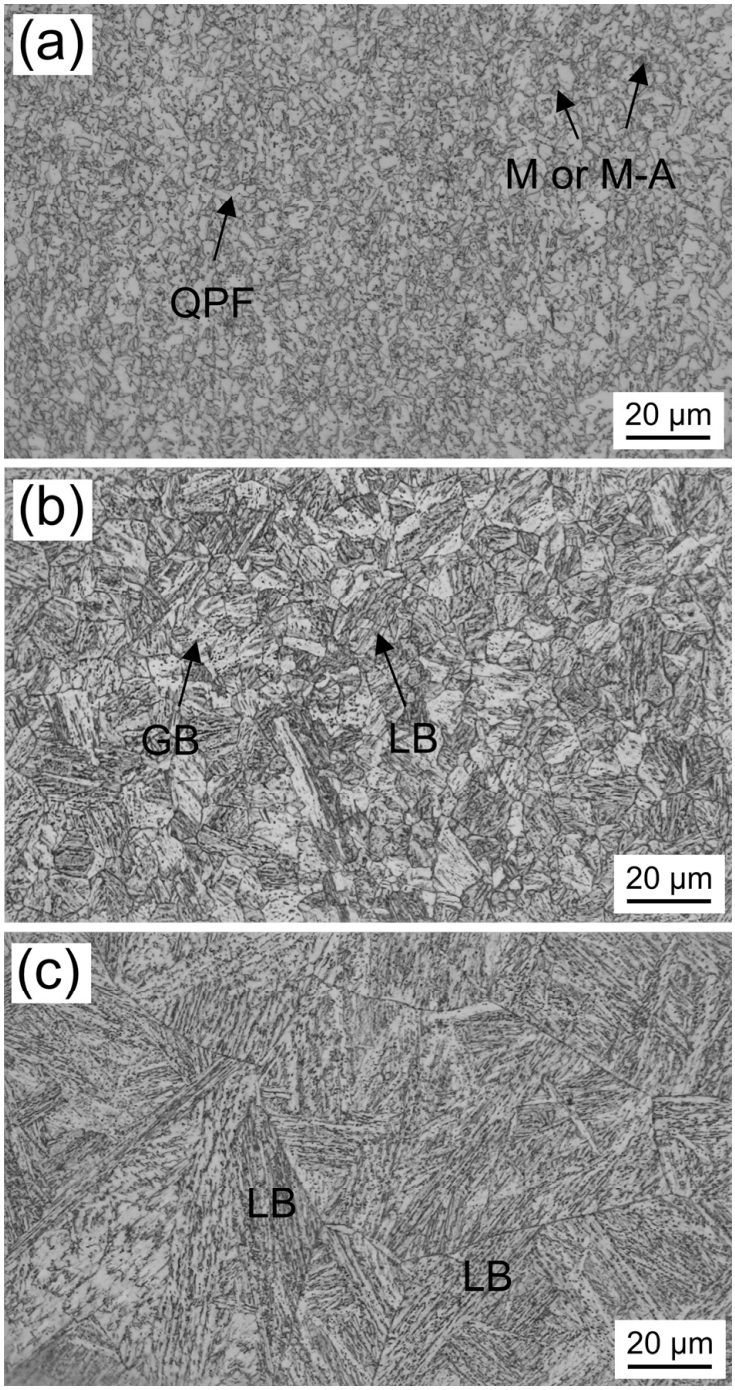


Figure 2. Typical micrographs of the experimental steel with different austenitizing temperatures: (**a**) 860 °C; (**b**) 1000 °C; (**c**) 1250 °C (M: martensite; M-A: martensite-austenite constituent; QPF: quasi-polygonal ferrite; LB: lath bainite; GB: granular bainite).

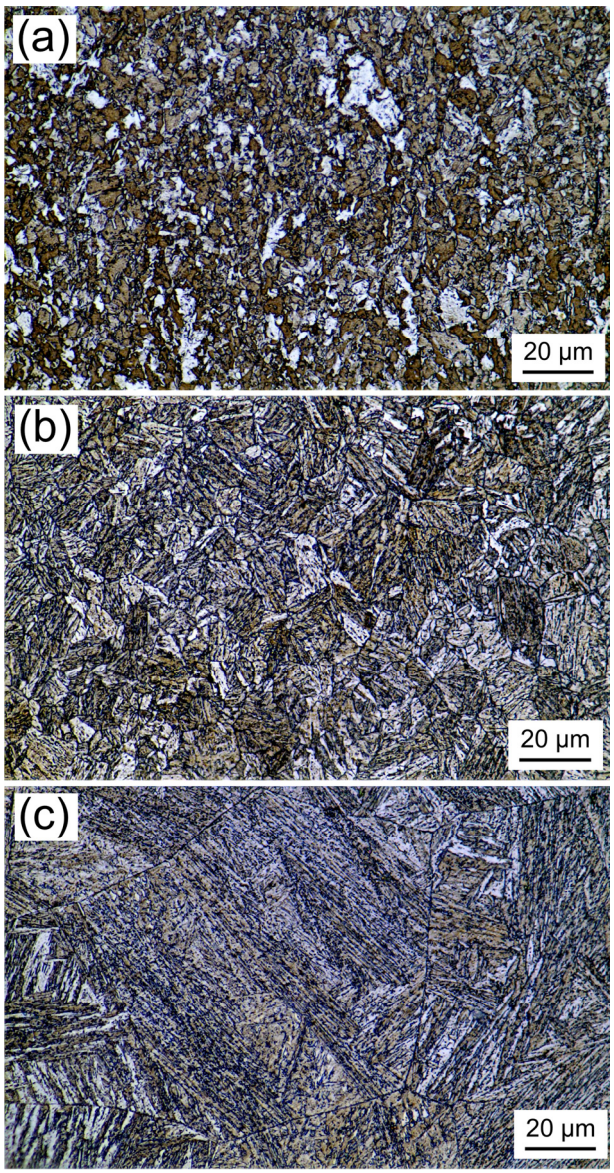


Figure 3. Distribution and morphology of the M-A (white) etched by LePera reagent with different austenitizing temperatures: (**a**) 860 °C; (**b**) 1000 °C; (**c**) 1250 °C.

3.2. Expansion Curve

Figure 4 shows the expansion curves for the lengths of the specimens treated with different austenitizing temperatures at a cooling rate of 10 °C/s. The bainite starting (B_s) and bainite finishing (B_f) temperatures were considered to be the temperatures corresponding to the deviation points of the thermal expansion lines of austenite and bainite on the expansion curves [10]. In Figure 4, the arrows show the B_s and B_f temperatures of the sample at the austenitization temperature of 860 °C. The measured B_s temperature in the specimen austenitized at 860 °C is approximately 606 °C. The theoretical B_s was calculated to be about 642 °C using Equation (1) proposed by van Bohemen [25]. The theoretical B_s is higher than the experimentally determined one because incubation is required to start the transformation. It is observed that the austenitizing temperature obviously affects the bainite transformation.

$$B_s = 839 - 86x_{Mn} - 23x_{Si} - 67x_{Cr} - 33x_{Ni} - 75x_{Mo} \\ -270[1 - exp(-1.33x_C)] \quad (1)$$

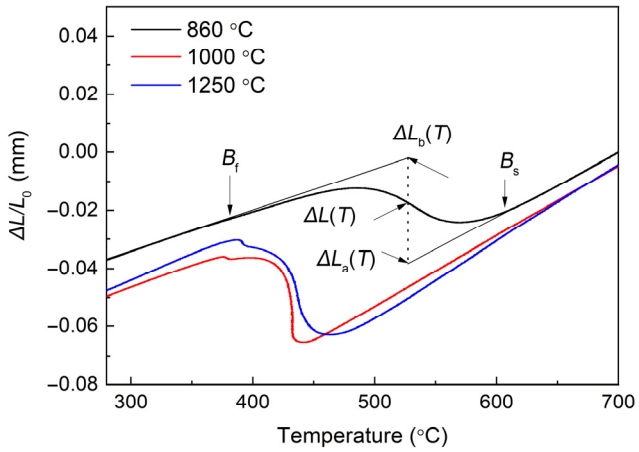


Figure 4. Expansion curves for the experimental steel subjected to different austenitizing temperatures.

The B_s and B_f temperatures of the specimens treated with an austenitizing temperature of 1000 °C are lower than the specimens treated with 860 °C and 1250 °C. This phenomenon is more pronounced for the B_s temperature than that for the B_f. The austenitizing temperature of 1000 °C is lower than the austenite coarsening temperature of the experimental steel, so the austenitic grains grow without obvious coarsening and the austenite grains are finer. According to the shear mechanism for bainitic transformation, the bainite nucleus are formed by the separation of original dislocations. Fine austenite grains with high density of dislocation retard the bainite nucleation by inhibiting the mobility of incipient crystal with a body-centered cubic (BCC) structure. Consequently, higher supercooling is required to compensate for the higher driving forces associated with the phase transformation of fine austenite grains. This explains why the B_s in the sample austenitized at 1000 °C is lower than in that austenitized at 1250 °C. On the other hand, the relatively high B_s temperature in specimens treated at the lowest austenitizing temperature of 860 °C is due to the inhomogeneous chemical composition in the austenite. The solute-depleted region in austenite can promote the nucleation of the product phase [26]. Combining the information from Figures 2 and 4, polygonal ferrite first forms in the sample with the lowest austenitizing temperature (860 °C). This is because the stability of austenite decreases with the reduction of dissolved elements such as Mn, Si, Cr and Nb. During continuous cooling, the solute-depleted region in austenite may transform into polygonal ferrite. When the austenitizing temperature is 1250 °C, the AGS is coarse, which leads to a reduction in the bainitic nucleation sites. In addition, the complete dissolution and uniform distribution of alloying elements improve the stability of austenite. Therefore, its B_s temperature is relatively low. In summary, the B_s temperature and bainitic transformation temperature range of the specimen austenitized at 1000 °C is lower than those austenitized at 860 and 1250 °C.

3.3. Kinetics of Continuous Cooling Bainite Transformation

The volume fraction of the product phase ($f_v(T)$) can be calculated by Equation (2) using the classical lever rule and based on the dilatation curve, as shown in Figure 4. In the above equation, $\Delta L(T)$ is the actual value of the length change of the specimen at the temperature of T, and $\Delta L_a(T)$ and $\Delta L_b(T)$ can be obtained by extrapolating the linear thermal expansion of the fully austenite and bainite at the temperature of T, respectively.

$$f_v(T) = \frac{\Delta L(T) - \Delta L_a(T)}{\Delta L_b(T) - \Delta L_a(T)} \quad (2)$$

Figure 5 illustrates the bainite kinetic curves for the experimental steel. It is assumed that austenite is completely transformed to bainite. Although residual austenite may be present in the transformation products, the volume fraction of residual austenite is small

and negligible in the calculations. The shape of the transformation curve is determined by the temperature and driving force of phase transformation. As the temperature of phase transformation decreases, the supercooling degree and driving force increase, but the ability of carbon diffusion decreases. Therefore, the fastest transformation rate of bainitic transformation occurs at the mid-temperature [27].

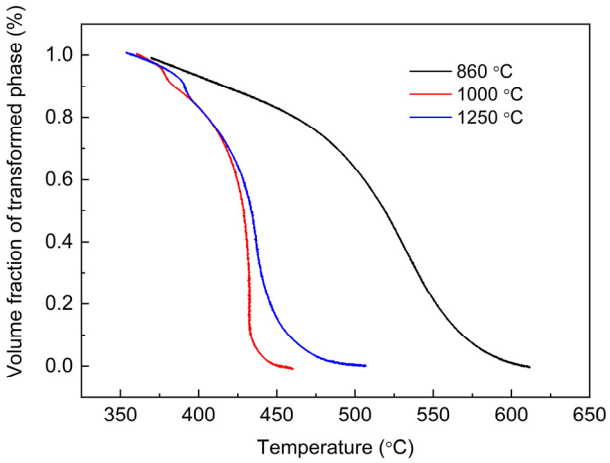


Figure 5. Kinetic curves of bainite transformation in the experimental steel treated with different austenitizing temperatures.

The effect of AGS on bainitic transformation is non-monotonic. The bainite transformation kinetics of the sample austenitized at 1000 °C was significantly accelerated compared to that austenitized at 860 °C. However, when the austenitising temperature rises to 1250 °C, the transformation kinetics is no longer accelerated further. It is well known that AGS increases with increasing austenitising temperature, so it can be inferred that there is a critical AGS, below which the effect of AGS on the bainitic transformation kinetics is significant, whereas above which this effect is weak. The maximum length of bainite sheaves equals the diameter of prior austenite because the growth of bainite is limited by the prior austenite grains. There are a lot of grain boundary nucleation of bainite and the event of hard impingement is very frequent when the AGS is below the critical value. If the AGS is above the critical value, the nucleation density of bainite decreases and the impingement event between bainite sheaves decreases.

Transformation kinetic curves further indicate that the austenite grain in the sample austenitized at 1000 °C reduces the bainite transformation temperature ranges. And the length of bainite sheaves obtained from the sample austenitized at 1000 °C is close to the diameter of AGS (see Figure 2). Furthermore, the phase transformation rate of the specimen with an austenitizing temperature of 860 °C decreases significantly near the intermediate stage of transformation, which is mainly caused by the enrichment of carbon in austenite discharged from polygonal ferrite. Thus, the phase transformation kinetics are influenced to some extent by the diffusion of carbon at the end of the phase transformation [28,29].

Figure 6 illustrates the variation of the bainite reaction rate with different austenitizing temperatures. It is observed that the effect of AGS on transformation rate is non-monotonic. The reaction rate of the specimen austenitized at 1000 °C is higher than those at 1250 and 860 °C. There was no significant coarsening of the AGS in the 1000 °C austenitized specimen compared to the 860 °C austenitized specimen, as described above, and therefore the nucleation sites of bainite were not significantly reduced. However, the driving force for bainite transformation was obviously larger in the specimen austenitized at 1000 °C due to lower transformation temperature, which results in the acceleration of bainite transformation. On the other hand, the transformation temperature in the specimen austenitized at 1000 °C was slightly lower than that austenitized at 1250 °C, and the preferential nucleation sites are expected to be larger in the former one because AGS

obviously coarsens at 1250 °C (Figure 2). In addition, transformation stasis can be observed at the beginning of transformation (marked by arrow 1 in Figure 6) in the specimen austenitized at 1000 °C. This is mainly due to the solid solution drag of elements Ti and Nb at the bainite/austenite interface, inhibiting the bainite nucleation. At the beginning of the bainite transformation, the phase transformation temperature is relatively high and the solid-solution drag effect between atoms Ti, Nb and C is more likely to impede the movement of the phase interface, which can be identified by the reduction of the phase transformation rate. After the precipitation of (Ti, Nb)C, the solid-solution drag effect diminishes or disappears, and the migration of the phase interface is reactivated again. Moreover, another peak in the transformation rate curves occurs at the end stage of the transformation (marked by arrows 2 and 3 in Figure 6). Gupta et al. [30] believes that the formation of interplate precipitates or secondary M-A components leads to the emergence of the second peak. Reisinger et al. [31] also found a two-stage transformation behavior in a CrMoV steel. They stated that the carbon enrichment in austenite led to a stasis of the transformation. As the temperature decreased, the transformation onset again at the second stage. In the present study, the second peak may correspond to the formation of martensite because it appears at low temperatures below 400 °C.

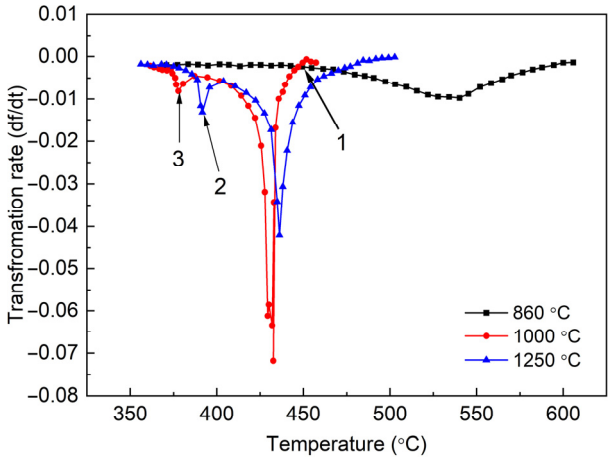


Figure 6. Phase transformation rate versus cooling temperature for the experimental steel at different austenitization temperatures. Arrow 1 indicates the transformation stasis at the beginning of transformation. Arrows 2 and 3 indicate the second peak in the transformation rate curves.

The rate of phase transformation is closely related to the nucleation, growth and impingement of the product phase. Grain boundaries and the already formed bainite lath are the main positions for bainite nucleation, which can be seen from the microstructure in Figure 2. The morphology of the parallel lath structure exhibits a high degree of anisotropy and one-dimensional growth. By contrast, polygonal ferrite tends to transform at a constant nucleation rate and in two-dimensional or three-dimensional growth at a slower cooling rate. Song et al. [32] proposed an analytical model to determine the kinetic information by analyzing the maximum transformation rate and they summarized that the impingement mode of the isochronous phase transition can be determined by the position of the maximum transformation rate.

According to Figures 5 and 6, the location of the peak transformation rate occurs near 50% of the transformation volume fraction at the cooling rate of 10 °C /s, which indicates that the prevalent type of impingement mode is anisotropic growth impingement as the volume fraction of the transformation at the peak rate location is less than 0.632 [32]. Obviously, this result is also well corroborated by the microstructure morphology described above.

4. Conclusions

The effect of austenitizing temperature on the transformation kinetics and microstructure of a low-carbon bainite steel was investigated in the present study. The following conclusions can be drawn.

(1) The morphology of the microstructure changes from polygonal ferrite and granular bainite to lath bainite as the austenitizing temperature of the multi-functional structural steel is increased from 860 to 1250 °C, and the average grain size of austenite is increased from 7 to 62 μm.
(2) The B_s temperature and bainitic transformation temperature range of the specimen austenitized at 1000 °C is lower than those austenitized at 860 and 1250 °C.
(3) Bainite transformatioin rate is influenced by the nucleation and growth of bainite. As the austneite grain size increases, the number of nucleation sites decreases, but the growth of bainite is promoted. It is found that the growth of bainite is more important in determining the transformation rate than the nucleation in the 690 MPa microalloyed multi-functional structural steel.
(4) For the novel high-strength multi-functional structural steel, there is a critical austenite grain size. Below the critical value, the effect of austenite grain size on the bainitic transformation is significant, whereas this effect is weak above the critical value.

Author Contributions: Z.C., conceived and designed the experiments; X.Z., conducted experiments and analyzed the data; J.Q., analyzed the experimental data; W.Z., conducted experiments and analyzed the data; Y.Z., conducted experiments; L.C., conceived the experiments. All authors participated in the discussion of experimental results. All authors have read and agreed to the published version of the manuscript.

Funding: The authors gratefully acknowledge the financial supports from the Key Research and Development Program of Hebei Province of China (Grant No. 18211019D) and "333 Talent Project" of Hebei (Grant No. A201803007).

Conflicts of Interest: The authors declare no conflict of interest. The founding sponsors had no role in the design of the study; in the collection, analyses, or interpretation of data; in the writing of the manuscript; or in the decision to publish the results.

References

1. Bjorhovde, R. Performance and design issues for high strengthsteel in structures. *Adv. Struct. Eng.* **2010**, *13*, 403–411. [CrossRef]
2. Ishii, T.; Fujisawa, S.; Ohmori, A. Overview and application of steel materials for high-rise buildings. *JFE Tech. Rep.* **2009**, *14*, 1–8. [CrossRef]
3. Li, G.Q.; Wang, Y.B.; Chen, S.W.; Sun, F.F. State-of-the-art on research of high strength structural steels and key issues of using high strength steels in seismic structures. *J. Build. Struct.* **2013**, *34*, 1–13.
4. Zhang, Y.; Li, X.H.; Liu, Y.C.; Liu, C.X.; Dong, J.; Yu, L.M.; Li, H.J. Study of the kinetics of austenite grain growth by dynamic Ti-rich and Nb-rich carbonitride dissolution in HSLA steel: In-situ observation and modeling. *Mater. Charact.* **2020**, *169*, 110612. [CrossRef]
5. Xiong, W.M.; Song, R.B.; Huo, W.F.; Yu, P.; Qin, S.; Liu, Z.J. Microstructure characteristics and impact fracture mechanisms of Nb and V–Ti micro-alloyed offshore platform steels. *Vacuum* **2022**, *195*, 110709. [CrossRef]
6. Singh, A.P.; Pant, G. Mechanical behaviour of vanadium microalloyed steel under control environment compression. *Mater. Today Proc.* **2020**, *26*, 2525–2527. [CrossRef]
7. Zhang, Y.; Xu, Z.; Zhao, X.; Gao, G.; Hui, W.; Weng, Y. Hydrogen embrittlement behavior of high strength bainitic rail steel: Effect of tempering treatment. *Eng. Fail. Anal.* **2018**, *93*, 100–110. [CrossRef]
8. Girault, E.; Jacques, P.; Ratchev, P.; Humbeeck, J.V.; Verlinden, B.; Aernoudt, E. Study of the temperature dependence of the bainitic transformation rate in a multiphase TRIP-assisted steel. *Mater. Sci. Eng. A* **1999**, *s273–s275*, 471–474. [CrossRef]
9. Umemoto, M.; Horiuchi, K.; Tamura, I. Transformation kinetics of bainite during isothermal holding and continuous cooling. *Trans. Iron Steel Inst. Jpn.* **1981**, *22*, 854–861. [CrossRef]
10. Lee, S.J.; Park, J.S.; Lee, Y.K. Effect of austenite grain size on the transformation kinetics of upper and lower bainite in a low-alloy steel. *Scr. Mater.* **2008**, *59*, 87–90. [CrossRef]
11. Lan, L.Y.; Qiu, C.L.; Zhao, D.W.; Gao, X.H.; Du, L.X. Effect of austenite grain size on isothermal bainite transformation in low carbon microalloyed steel. *Mater. Sci. Technol.* **2011**, *27*, 1657–1663. [CrossRef]

12. Li, Z.Y.; Li, P.F.; Luo, Y.; Zhou, X.Y.; Qi, L.; Li, S.C.; Wang, Z.G. Effect of Austenitizing Temperature and Prior Martensite on Ultra-Fine Bainite Transformation Kinetics. *Metals* **2019**, *9*, 1309. [CrossRef]
13. Xu, G.; Liu, F.; Wang, L.; Hu, H. A new approach to quantitative analysis of bainitic transformation in a superbainite steel. *Scr. Mater.* **2013**, *68*, 833–836. [CrossRef]
14. Hu, F.; Hodgson, P.D.; Wu, K.M. Acceleration of the super bainite transformation through a coarse austenite grain size. *Mater. Lett.* **2014**, *122*, 240–243. [CrossRef]
15. Hasan, S.M.; Kumar, S.; Chakrabarti, D.; Singh, S.B. Effect of prior austenite grain size on the formation of carbide-free bainite in low-alloy steel. *Philos. Mag.* **2020**, *100*, 2320–2334. [CrossRef]
16. Matsuzaki, A.; Bhadeshia, H.K.D.H. Effect of austenite grain size and bainite morphology on overall kinetics of bainite transformation in steels. *Mater. Sci. Technol.* **2013**, *15*, 518–522. [CrossRef]
17. Wei, W.; Retzl, P.; Kozeschnik, E.; Povoden-Karadeniz, E. A semi-physical α-β model on bainite transformation kinetics and carbon partitioning. *Acta Mater.* **2021**, *207*, 116701. [CrossRef]
18. Ravi, A.M.; Kumar, A.; Herbig, M.; Sietsma, J.; Santofimia, M.J. Santofimia. Impact of austenite grain boundaries and ferrite nucleation on bainite formation in steels. *Acta Mater.* **2020**, *188*, 424–434. [CrossRef]
19. Song, C.H. Investigation of microstructural evolution and bainite transformation kinetics of multi-phase steel. *Mater. Sci. Eng. A* **2019**, *774*, 138868.
20. Asga, B.; Na, A. Effects of prior austenite grain size and phase transformation temperature on bainitic ferrite formation in multi-constituent microstructures of a strong ultra-low-carbon steel. *Mater. Sci. Eng. A* **2021**, *815*, 141300.
21. Zhu, W.T.; Cui, J.J.; Chen, Z.Y.; Feng, Y.; Zhao, Y.; Chen, L.Q. Design and performance of 690 MPa grade low-carbon microalloyed construction structural steel with high strength and toughness. *Acta Metall. Sin.* **2021**, *57*, 340–352.
22. Wang, T.; Qian, L.; Yu, W.; Li, K.; Zhang, F.; Meng, J. Effect of ferrite-austenite morphology and orientation relationship on bainite transformation in low-alloy TRIP steels. *Mater. Charact.* **2022**, *184*, 111656. [CrossRef]
23. Zhang, M.; Wang, Y.H.; Zheng, C.L.; Zhang, F.C.; Wang, T.S. Austenite deformation behavior and the effect of ausforming process on martensite starting temperature and ausformed martensite microstructure in medium-carbon Si–Al-rich alloy steel. *Mater. Sci. Eng. A* **2014**, *596*, 9–14. [CrossRef]
24. Mondal, J.; Das, K.; Das, S. Isothermal transformation kinetics, microstructure and mechanical properties of a carbide free bainitic steel. *Mater. Charact.* **2021**, *177*, 111166. [CrossRef]
25. van Bohemen, S.M.C. Bainite and martensite start temperature calculated with exponential carbon dependence. *Mater. Sci. Technol.* **2013**, *28*, 487–495. [CrossRef]
26. An, F.C.; Zhao, S.X.; Xue, X.K.; Wang, J.J.; Yuan, G.; Liu, C.M. Incompleteness of bainite transformation in quenched and tempered steel under continuous cooling conditions. *J. Mater. Res. Technol.* **2020**, *9*, 8985–8996. [CrossRef]
27. Hu, H.J.; Xu, G.; Zhang, Y.L.; Xue, Z.L.; Zhou, M.X. Dynamic observation of bainite transformation in a Fe-C-Mn-Si superbainite steel. *J. Wuhan Univ. Technol. Mater. Sci. Ed.* **2015**, *30*, 818–821. [CrossRef]
28. Varshney, A.; Sangal, S.; Pramanick, A.K.; Mondal, K. On the extent of transformation of austenite to bainitic ferrite and carbide during austempering of high Si steel for prolonged duration and its effect on mechanical properties. *Mater. Sci. Eng. A* **2020**, *793*, 139764. [CrossRef]
29. Chen, H.; Zhu, K.Y.; Zhao, L.; van der Zwaag, S. Analysis of transformation stasis during the isothermal bainitic ferrite formation in Fe-C-Mn and Fe-C-Mn-Si alloys. *Acta Mater.* **2013**, *61*, 5458–5468. [CrossRef]
30. Gupta, C.; Dey, G.K.; Chakravartty, J.K.; Srivastav, D.; Banerjee, S. A study of bainite transformation in a new CrMoV steel under continuous cooling conditions. *Scr. Mater.* **2005**, *53*, 559–564. [CrossRef]
31. Reisinger, S.; Kozeschnik, E.; Ressel, G.; Keckes, J.; Stark, A.; Marsoner, S.; Ebner, R. Strain energy contributions on the bainitic phase transformation in a CrMoV steel during continuous cooling. *Mater. Des.* **2018**, *155*, 475–484. [CrossRef]
32. Song, S.J.; Liu, F.; Jiang, Y.H. Impact of anisotropic growth on kinetics of solid-state phase transformation. *Trans. Nonferrous Met. Soc. China* **2012**, *22*, 895–900. [CrossRef]